Europe PMC Funders Group
Author Manuscript
Nat Catal. Author manuscript; available in PMC 2020 September 02.

Published in final edited form as:
Nat Catal. 2020 April ; 3(4): 376–385. doi:10.1038/s41929-020-0431-3.

Nanostructuring unlocks high performance of platinum single-atom catalysts for stable vinyl chloride production

Selina K. Kaiser[#1], **Edvin Fako**[#2], **Gabriele Manzocchi**[1], **Frank Krumeich**[1], **Roland Hauert**[3], **Adam H. Clark**[4], **Olga V. Safonova**[4], **Núria López**[2], **Javier Pérez-Ramírez**[1,*]

[1]Institute for Chemical and Bioengineering, Department of Chemistry and Applied Biosciences, ETH Zurich, Vladimir-Prelog-Weg 1, 8093 Zurich, Switzerland [2]Institute of Chemical Research of Catalonia (ICIQ), The Barcelona Institute of Science and Technology, Av. Països Catalans 16, 43007 Tarragona, Spain [3]Empa, Swiss Federal Laboratories for Materials Science and Technology, Überlandstrasse 129, 8600 Dübendorf, Switzerland [4]Paul Scherrer Institut, 5232 Villigen PSI, Switzerland

[#] These authors contributed equally to this work.

Abstract

A worldwide replacement of the toxic mercuric chloride catalyst in vinyl chloride manufacture *via* acetylene hydrochlorination is slowed down by the limited durability of alternative catalytic systems at high space velocities. Here, we demonstrate that platinum single atoms on carbon carriers are substantially more stable (up to 1073 K) than their gold counterparts (up to 473 K), enabling facile and scalable preparation and precise tuning of their coordination environment by simple temperature control. By combining kinetic analysis, advanced characterisation, and density functional theory, we assess how the Pt species determines the catalytic performance and thereby identify Pt(II)−Cl as the active site, being three times more active than Pt nanoparticles. Remarkably, we show that Pt single atoms exhibit outstanding stability in acetylene hydrochlorination and surpass the space-time-yields of their gold-based analogues after 25 h time-on-stream, qualifying as candidate for sustainable vinyl chloride production.

Users may view, print, copy, and download text and data-mine the content in such documents, for the purposes of academic research, subject always to the full Conditions of use:http://www.nature.com/authors/editorial_policies/license.html#terms

Correspondence and requests for materials should be addressed to J.P.-R.

Data availability
The data that support the plots within this paper and other findings of this study are available from the corresponding author upon reasonable request. The DFT structures can be retrieved from the ioChem-BD database.[56]

Author contributions
J.P.-R. conceived and coordinated all stages of this research. S.K.K. prepared and characterised the catalysts, and performed and analysed the steady-state tests with support from G.M.. E.F. and N.L. conducted the DFT calculations. F.K. performed the microscopic analysis. R.H. conducted the XPS analysis. O.V.S. and A.C. conducted the XAS analysis. The data were discussed among all the authors. S.K.K., E.F., and J.P.-R. wrote the paper with feedback from the other authors.

Competing interests
The authors declare that they have no competing interests.

Reprints and permissions information is available at (link).

Publisher's note: Springer Nature remains neutral with regard to jurisdictional claims in published maps and institutional affiliations.

Europe PMC Funders Author Manuscripts
Europe PMC Funders Author Manuscripts

Europe PMC Funders Author Manuscripts

Europe PMC Funders Author Manuscripts

Single-atom heterogeneous catalysts (SACs), containing spatially isolated metal atoms stabilised on appropriate hosts, have emerged as a promising class of materials with diverse applications in chemical transformations[1–5] and energy conversion.[6–8] Owing to the increased active site uniformity and the possibility to tune the coordination environment through adapting the host structure,[9–13] SACs are uniquely suited to derive structure-performance relationships and gain mechanistic understanding of complex catalytic transformations, a prerequisite for the design of high-performance catalysts, needed to meet the sustainability goals of modern society.[14]

A prominent example is vinyl chloride manufacture *via* acetylene hydrochlorination, a long-established industrial process which runs over highly toxic and volatile mercury-based catalysts, causing severe consequences for human health and the environment.[15–17] For the transition into a sustainable process, an economically viable alternative catalyst is imperative.[18] To this end, carbon-supported gold and ruthenium-based catalysts have emerged as the most promising candidates, reaching significant activity, thanks to recent advancements in the precise control of their atomic architecture.[19–21] While Au(I)−Cl single atoms have been identified as the active site in gold catalysts, their nanoparticle-based counterparts are virtually inactive.[9,22–24] Interestingly, the opposite particle-size dependency was found for ruthenium catalysts, underlining the importance of careful nanostructuring of the active site.[25] Despite promising initial activity, both metal-based catalysts suffer from deactivation, mainly due to reduction of the active metal sites and agglomeration (*i.e.*, on non-functionalised carbon supports), or fouling (*i.e.*, on functionalised carbon supports).[9,17,23,25] In order to improve the catalyst stability, several strategies, some of which have reached pilot plant testing,[20,26] have been developed, based on employing organic ligands containing soft donor atoms (*e.g.* thiosulfate, thiocyanate, thiourea, and cyanides to stabilise cationic Au),[20,26] ionic liquids,[21] additional metals and/or promoters,[16,17,27] and functionalised supports (*i.e.*, N, S, P, B-doped carbons or carbon-metal oxide mixtures).[17,24] In particular, the former approach led to the commercialisation of an activated carbon (AC) supported gold catalyst modified with thiosulphate ($(NH_4)_2Au(S_2O_3)_3$/AC),[20] but to date, no process installation has been publicly announced. A possible limitation may be the lack of intrinsic catalyst stability. Since durability tests in acetylene hydrochlorination are commonly conducted at very mild conditions, applying low gas hourly space velocities (*GHSV*(C_2H_2) of <100 h^{-1} based on acetylene) or an excess of catalyst leading to acetylene conversions of 100%, it is unfeasible to evaluate and compare the intrinsic stability of reported state-of-the-art systems. Alternatively, the identification of other active metal sites, which can be sufficiently stabilised by the oxygen-functionalities present in the relatively fouling-resistant activated carbon carrier,[9] could lead to the development of robust hydrochlorination catalysts. In this regard, platinum is a potentially promising candidate as it interacts very strongly with the surface oxygen groups of a broad range of metal oxide supports (*i.e.*, CeO_2)[4,29–32] and additionally features a more flexible coordination chemistry with respect to gold.[33] Notably, Pt also exhibits a *ca.* 40% lower price compared to Au,[28] rendering it appealing from an industrial perspective. However, to date there are only a few studies on Pt-based catalysts for acetylene hydrochlorination,[27,34–36] likely due to the *ca.* 7 times lower catalytic activity compared to Au-based systems, which might have discouraged detailed investigations into this metal. On the other hand, nanostructuring of the active site

Europe PMC Funders Author Manuscripts

Europe PMC Funders Author Manuscripts

has been proven pivotal for the success of gold and ruthenium-based catalysts, suggesting that also platinum may unfold considerable potential in acetylene hydrochlorination if nuclearity and host effects are optimally orchestrated.

Herein, we evaluate the properties and host effects of single-atom Pt catalysts for acetylene hydrochlorination. For this purpose, we design a platform of Pt SACs with tunable coordination environment (−Cl, −N neighbours) and oxidation state (II and IV), by functionalising the carbon support and using controlled thermal activation. Analogous to gold catalysts, we demonstrate that platinum single atoms exhibit superior catalytic activity and stability in acetylene hydrochlorination with respect to their nanoparticle-based counterparts. While the catalytic response is not affected by the choice of the carbon support (activated carbon or nitrogen-doped carbon), the latter determines the stability under reaction conditions. Specifically, pyrrolic-N sites were identified to promote a coking mechanism as rationalised by density functional theory (DFT). In direct comparison to Au/AC single-atom catalysts, which inexorably deactivate, Pt/AC SACs maintain a stable performance for 100 h, surpassing the space-time-yields of the former within only 25 h time-on-stream. The origin of these differences is analysed by combining X-ray photoelectron spectroscopy (XPS), X-ray absorption spectroscopy (XAS), and scanning transmission electron microscopy (STEM) with mechanistic studies based on DFT.

Results

Stability of platinum *versus* gold single atoms on carbon carriers

Carbon-supported platinum nanostructures ranging from single atoms to nanoparticles at a fixed metal loading (1 wt.%) were derived *via* a two-step synthesis,[9,22] comprising the incipient wetness impregnation of activated carbon (AC) or polyaniline-derived N-doped carbon (NC) with a solution of H_2PtCl_6 dissolved in water (w) or aqua regia (a), followed by drying (static air, 473 K), and thermal activation at distinct temperatures (T_{act}, 16 h, N_2 atmosphere), which yielded three series of Pt based catalysts Pt/AC-a-T_{act}, Pt/AC-w-T_{act}, and Pt/NC-w-T_{act} (Figure 1a, Supplementary Table 1). The thermal activation was conducted in the range of 473-1073 K, in order to avoid changes to the catalysts upon exposure to the reaction temperature of acetylene hydrochlorination (T_{bed} = 473 K) and not exceed the carbonisation temperature of the N-doped carbon support (1073 K), preserving the total nitrogen content and speciation over the whole temperature range, as confirmed by N 1*s* XPS analysis (Supplementary Figure 1). Remarkably, in all three low-temperature platinum catalysts (T_{act} = 473 K), the metal was atomically dispersed, as evident from STEM images and corroborated by the absence of platinum diffraction peaks in the XRD spectra (Figure 1a, Supplementary Figures 2-5). The synthetic simplicity of deriving carbon-supported platinum single atoms is a clear advantage over the harsh reaction conditions required to atomically disperse gold (*i.e.*, aqua regia as impregnation solvent).[9] In addition, Pt single atoms exhibit superior thermal stability, remaining atomically dispersed up to 1073 K on AC, while gold single atoms readily agglomerate above 473 K, if not stabilised by suitable metal anchoring sites such as nitrogen-containing functional groups.[9] Notably, the choice of impregnation solvent affects the thermal stability of Pt single atoms on AC, hinting at a decisive role of the surface functionalisation of the carrier. In particular, the surface

Europe PMC Funders Author Manuscripts

Europe PMC Funders Author Manuscripts

oxygen and chlorine contents (Table 1), as derived from XPS analysis, differ markedly between the water-impregnated (4.2 at.% O and 0.2 at.% Cl in Pt/AC-w-473) and the aqua regia-treated sample (7.1 at.% O and 0.8 at.% Cl in Pt/AC-a-473). Besides the carrier functionalisation, also the nature of the Pt site is directly affected by the solvent choice, as analysed by combining XPS and XAS analysis (Figures 1b,c, Supplementary Figures 6-8 and Supplementary Tables 2-4). Fitting of the XPS spectra of the low-temperature water-based samples, Pt/AC w-473 and Pt/NC w-473 revealed a significant contribution at a binding energy (*B.E.*) of 72.4 ±0.1 eV that is commonly assigned to Pt(II).[37] In aqueous solution H_2PtCl_6 undergoes fast hydrolysis, during which chloride ions are exchanged for water molecules.[38] In the subsequent impregnation step, the Pt(IV) species (*i.e.*, $[PtCl_{6-x}(H_2O)_x]^{-2+x}$) is partially reduced to Pt(II) on the carbon support.[39] The low-temperature aqua regia-based sample (Pt/AC-a-473) exhibits a major contribution at a binding energy of *B.E.* = 73.6 ±0.1 eV, indicating differences in the coordination environment (*i.e.*, additional Cl-neighbours) with respect to the water-based samples and/or a formally higher oxidation state, which can be tentatively assigned to Pt(IV).[37,40] In good agreement with these results, the extended X-ray adsorption fine structure (EXAFS) analysis of Pt/NC-w-473, Pt/AC-w-473, and Pt/AC-a-473 indicates 2.3±0.3, 3.2±0.3, and 3.8±0.2 Cl-neighbours, respectively (Supplementary Table 4). Notably, no peaks characteristic for Pt−Pt bonds were detected for the low-temperature samples, corroborating the atomic dispersion of platinum as visualised by STEM. With increasing thermal activation temperature, the coordination environment of the Pt single atoms in the Pt/NC-w-T_{act} and the Pt/AC-a-T_{act} series gradually changes from predominantly Cl to O/N-neighbouring atoms (*i.e.*, 0.7±0.1 Cl and 2.2±0.2 O/N-neighbours in Pt/NC-w-673 and 0.2±0.1 Cl and 2.5±0.1 O/N-neighbours in Pt/NC-w-1073). Besides, fitting of the first coordination shell further revealed a small Pt−Pt contribution with a coordination number (CN) of 1±0.4 (Pt-foil CN = 12) at a slightly enlarged coordination shell distance (*R*) of 2.93±0.01 Å (Pt-foil: *R* = 2.76 Å),[41] possibly indicating the presence of low-nuclearity Pt-N/O clusters (*i.e.*, dimers, trimers) in Pt/NC-w-1073 and Pt/AC-a-1073. For Pt/AC w 1073, a clear contribution of Pt(0) (*B.E.* = 71.2 eV)[37,40] is observed in XPS, which agrees well with the presence of nanoparticles, as visualised by STEM (Supplementary Figure 3).

To rationalise the remarkable stability of Pt single atoms and their evolution during thermal activation on the carbon carriers with respect to their Au-based analogues (Figure 2a), DFT studies were performed. The NC and AC supports were represented by a set of basal (and sp^3) defects containing different nitrogen and oxygen functionalities.[9] In order to evaluate the interaction between the set of defects and the possible single-atom species, a screening of formation energies was performed, using the blank metal atom, M, and the metal chloride, MCl, (M = Au, Pt) as probes. Two general trends were identified: (*i*) N-containing defects form stronger bonds to Pt and Au species, with respect to their O-containing analogues and (*ii*) Pt (or PtCl) species bind up to three times more strongly to the support than their Au (or AuCl) counterparts, regardless of the type of defect (O- or N-containing, Figures 2b,c, Supplementary Figure 9). Consequently, the stabilisation of Au single atoms on O-containing defects, is not sufficient to prevent their agglomeration at elevated temperatures, while Pt single atoms exhibit superior stability on both carbon carriers (AC and NC), if suitable oxygen and/or nitrogen-functionalities are provided. The preferred single-atom

Europe PMC Funders Author Manuscripts

Europe PMC Funders Author Manuscripts

species (M or MCl) depends for both metals on the geometry of the individual defects. Specifically, MCl species are preferred on all defects, except those which allow a square planar geometry of the metal site M. The latter enable the metal atom to adopt the in-plane position in the centre of the cavities (*i.e.*, −0.23 eV for Au and −2.59 eV for Pt in the 4×N6 cavity, with respect to the metal bulk reference), yielding configurations corresponding to Au(III) and Pt(II), respectively. The migration of SA species to these highly stable configurations is promoted by the removal of Cl that occurs at high catalyst activation temperatures.

Activity descriptors for platinum catalysts

Acetylene hydrochlorination over the three series of Pt catalysts was studied at bed temperatures (T_{bed}) of 423 – 523 K with a gas hourly space velocity based on acetylene ($GHSV(C_2H_2)$) of 1500 h^{-1} (Figure 3a). Analogous to the respective gold-based systems, 473 K was identified as the optimal reaction temperature and applied in all catalytic tests (Supplementary Figure 10a).[9] Notably, vinyl chloride monomer (VCM) was the only product detected in all tests by mass spectrometry (MS) analysis, as also commonly found for gold-based systems. Hence, the activity of Pt and Au-based catalysts is directly represented and compared as the yield of VCM (Y(VCM). The catalytic activity of the Pt/AC-w-T_{act} series markedly drops with increasing platinum mean particle size, indicating that alike gold, also platinum single atoms exhibit superior activity in comparison to their nanoparticle-based analogues (Figure 3b). Besides the metal particle size, also the metal oxidation state and the coordination environment of the single atoms strongly affect the performance (Figures 3c,d). Specifically, Pt(II)−Cl single atoms are *ca.* 2-fold more active than their Pt(IV)−Cl and Pt(II)−N(/O) analogues, yielding an overall activity hierarchy of: Pt(II)−Cl SA >> Pt(II)−N SA ≈ Pt(IV)-Cl SA > Pt(0) NPs. To gain a deeper understanding on the origin of these catalytic trends, we performed acetylene temperature-programmed desorption experiments (C_2H_2-TPD) with selected samples. In accordance to literature reports, Pt(II)-sites were found to exhibit a significantly higher adsorption capacity for acetylene compared to their Pt(IV) analogues (Supplementary Figures 11,12).[35] Besides the metal oxidation state, also the coordination environment of the single atoms affects their acetylene adsorption ability (Figure 3e). With an increase in N(/O)-neighbouring atoms the adsorption capacity gradually decreases, while no apparent changes in the adsorption strength were observed. In this regard, the superior catalytic activity of Pt(II)−Cl single atoms might be related to their relatively higher acetylene adsorption capacity in comparison to any other Pt-based site. Indeed, a correlation exists between the initial catalytic activity and the acetylene adsorption capacity of the Pt/NC-series (Figure 3f). Despite the importance of the coordination environment of the Pt single atoms, the catalytic response is independent of the choice of the carbon carrier (AC/NC) as long as the metal-site is unchanged (*i.e.*, Pt/AC-w-473, Pt/NC-w-473, Figure 3a). Overall, the optimised Pt SACs reach *ca.* half of the initial catalytic activity of state-of-the-art Au SACs, which is more than three times higher compared to the activity levels reported in literature for platinum-based catalysts, which were likely composed of Pt nanoparticles.[27,34,36]

Europe PMC Funders Author Manuscripts

Europe PMC Funders Author Manuscripts

Mechanistic studies

To gain atomistic insight into the structure-performance relationships of distinct Pt sites in acetylene hydrochlorination, DFT was employed. In addition to evaluating SA stability descriptors, (Supplementary Figure 9) the full set of empty and occupied (Pt and PtCl) defects was probed for acetylene adsorption, previously identified as a key indicator of activity.[9] As all considered Pt SA species have vacant coordination sites, acetylene adsorption was found to be highly exothermic over both the Pt and PtCl sites (up to −3.35 eV for a single Pt atom in a 3×N6 cavity) due to the formation of strong Pt−C bonds. The notable exception is the in-basal-plane square planar Pt(II) species, where the only contribution comes from van der Waals (vdW) interactions (Figures 4a,b). Due to the relatively high Cl to Pt ratio found in all catalysts (Table 1), the effect of incrementally closing the SA coordination sphere with Cl-ligands, on the acetylene adsorption ability was also evaluated. Since catalytic activity is a trade-off between stability and affinity towards the substrate, both were taken into consideration while identifying defects that are representative for the Pt/AC and Pt/NC catalysts, respectively (Supplementary Figures 13,14). A tri-pyrrolic (3×N5) defect was chosen for NC and a di-epoxide (2×Ep) for the AC system (Figures 4c,d). In both cases, closing the coordination sphere with additional chlorine ligands lowered the adsorption of acetylene, by reducing it from −2.29 eV (−2.85 eV) to −0.83 eV (−0.01 eV) for the Pt/NC (Pt/AC) system, accompanied by a corresponding increase in SA stability (Figures 4e,f). These results are well in line with the observed decrease in activity with increasing content of Pt (IV) species under reaction conditions (*vide infra*). Strong acetylene adsorption on Pt NPs was found to be the reason for their low activity, where acetylene effectively poisons the surface due to the fact that it is significantly more favoured than HCl (E_{ads}(HCl) = −1.03 eV, $E_{ads}(C_2H_2)$ = −2.78 eV, on Pt(111)). However, on MCl sites strong acetylene adsorption is favourable, since Cl is already coordinated to the metal centre, the reaction coordinate can advance *via* insertion of acetylene in-between Pt and Cl. This reduces the coordination of Pt and allows for the subsequent activation of HCl, followed by VCM evolution through a H transfer (Figure 5). Adsorption and subsequent activation of HCl as the first reaction step (Supplementary Figure 15) is less favourable as it leads to closing of the Pt coordination sphere and hence compromising acetylene affinity (Figure 4). This implies that anchored Pt (II) species with one or two Cl-neighbours should exhibit the highest performance in acetylene hydrochlorination. Since the Cl-coordination mainly governs site reactivity, similar behaviours can be expected for both low-temperature AC and NC SA catalysts (Pt/NC w-473 and Pt/AC w 473). The high affinity of Pt towards unsaturated C−C bonds leads to strong VCM adsorption (−1.82 eV), which is likely the main factor for the inferior catalytic activity of Pt SA catalysts compared to their Au SA (−1.23 eV) counterparts. Increasing the activation temperature of the NC and AC-supported Pt and Au catalysts, lowers the Cl-content and increases the population of the stable and inert basal-plane Pt(II)/Au(III) species. In principle, these sites can be activated by either HCl or acetylene, breaking two of the bonds to the support in order to form bonds with the substrate. However, this processes are endothermic (Supplementary Figure 16), rendering these sites undesirable for VCM evolution, and explaining their relatively low catalytic activity (*i.e.*, Pt/NC-w-1073).

Europe PMC Funders Author Manuscripts

Europe PMC Funders Author Manuscripts

Catalyst stability

To directly assess the stability of Pt and Au SACs as a function of the carbon carrier and compare their performance to state-of-the-art hydrochlorination catalysts (metal loading fixed to 1 wt.%), we conducted 30-70 h stability tests with Pt/AC-w-473, Pt/NC-w-473, Au/AC a-473, Au/NC-a-473, Ru/NC a 1073, and $(NH_4)_2Au(S_2O_3)_3$/AC (for simplicity denoted as Pt/AC, Pt/NC, Au/AC, Au/NC, Ru/NC, and Au-S/AC) under accelerated deactivation conditions, applying a *GHSV*(C_2H_2) of 650 h^{-1} (Figure 6a). Remarkably, Pt/AC shows a stable performance over the course of 70 h, which is in strong contrast to the gradual deactivation of Au/AC. The origin of this diverging behaviour lies in the intrinsic stability differences of gold and platinum single atoms on AC, while the former readily agglomerate due to a lack of suitable metal anchoring sites, platinum remains highly dispersed, as visualised by STEM analysis of the used catalyst (Figure 6b, Supplementary Figure 17).[9] Within *ca*. 25-h time on stream (*tos*), the activity of Au/AC drops below the conversion level of Pt/AC, demonstrating that Pt SACs are promising candidates for acetylene hydrochlorination. In view of potential industrial application, the possibility to derive stable Pt SACs *via* water-based impregnation is a significant advantage over the hazardous aqua regia-based synthesis protocol, commonly used to obtain Au SACs. Notably, the use of aqua regia can be avoided by employing sulphur-containing ligands (*i.e.*, thiosulphates),[20] but clearly the catalytic activity of the water-derived Au-S/AC system is inferior to the pristine Au/AC and Pt/AC catalysts. On N-doped carbon, the active site architecture is preserved for gold and platinum single atoms and graphene-confined Ru nanoparticles[25] under reaction conditions. However, the formation of carbonaceous residues accompanied by a gradual pore blockage and decrease in surface area, lowers the acetylene adsorption capacity with *tos*, likely being the premier reason for catalyst deactivation, regardless of the choice of metal (Supplementary Figures 12,18, Supplementary Table 6). Besides the porous properties, also the oxidation state of platinum and the coordination environment change under reaction conditions of acetylene hydrochlorination (Figures 1b,c). Specifically, the relative content of Pt(IV) quickly rises during the initial *tos* (60-80 at.%), accompanied by an increase in Cl neighbours (*i.e*, from 2.3±0.3 to 3.0±0.3 for Pt/NC, Supplementary Tables 2,4). In line with the relatively lower activity of Pt(IV)−Cl compared to Pt(II)−Cl, the catalytic activity initially drops, until the ratio of Pt(II)/Pt(IV) species is equilibrated and the reaction reaches a steady-state (Figure 6c, see Supplementary Discussion).

Origin of coke formation

To investigate the possible origin of the diverging coking tendency of activated carbon and N-doped carbon catalysts, we performed DFT calculations on the oligomerisation paths. Considering that the selectivity of all catalysts towards VCM was found to be 100%, it can be assumed that the H-termination process on the PtCl active sites is sufficiently fast to prevent the growth of longer hydrocarbon chains. Therefore, the key differences in the coking behaviour must have their origin in the structure of the carbon supports (AC/NC). In fact, the metal-free supports show the same diverging trends in their porous properties with *tos*, as their metal-based analogues (Supplementary Table 7, Supplementary Figure 12). The NC support contains a variety of N-heterocyclic moieties (Supplementary Table 3) of which the most abundant are the pyrrolic (N5), pyridinic (N6), and graphitic (N3) N-sites with *ca.*

Europe PMC Funders Author Manuscripts

Europe PMC Funders Author Manuscripts

50%, 30%, and 10% of the total N-content, respectively. The chemisorption of acetylene on a pristine graphitic surface (Figure 7a), or a graphitic-N (creating a 4-membered ring on the graphitic surface) is strongly hindered thermodynamically ($E_{ads}(C_2H_2)$ = 1.11 and 1.83 eV, respectively, Figure 7b). However, if a pyrrolic-N defect (**n1**, **h1**) is in close proximity, the chemisorption of acetylene triggers the opening of the 5 membered pyrrolic ring, allowing acetylene insertion and yielding a 7-membered ring. This process is highly exothermic ($E_{ads}(C_2H_2)$ = −2.02 and −3.42 eV, for **h1** and **n1**, respectively). Another acetylene molecule can be recurrently chemisorbed exothermically **(n1***, **h1***, Figure 7c). The presence of a PtCl species on NC enables parallel (kinetically less favourable) coking paths, including acetylene coupling and facilitated acetylene insertion into the pyrrolic ring (Supplementary Figure 19). On the contrary, on an O-rich defect the effect of acetylene chemisorption is significantly less pronounced ($E_{ads}(C_2H_2)$ = −0.30 eV, **k1**) and the main source of coking on AC is acetylene coupling over the initially predominating Pt(II) species (Supplementary Figure 19, red path, in contrast to the more stable Pt species on NC, purple path). In this regard, the individual coking characteristics mainly originate from the properties of the AC/NC supports.

Discussion

Nuclearity and host effects of carbon-supported platinum catalysts in acetylene hydrochlorination were systematically assessed by combining kinetic analysis, in-depth characterisation, and density functional theory studies, which enabled the identification of Pt(II)−Cl single atoms as the active site, achieving *ca.* 3 times higher activity than any previously reported Pt-based system. While acetylene readily poisons the surface of Pt nanoparticles, inhibiting HCl adsorption, on Pt(II)-Cl single atoms the adsorbed acetylene can be easily inserted in-between Pt and Cl, advancing the reaction coordinate. Additional Cl-ligands in the coordination sphere increase the stability of the single-atom site but lower the acetylene adsorption ability, which results in an overall decrease in catalytic activity, as observed during the initial *tos*. The choice of the carbon carrier (activated carbon or nitrogen-doped carbon) does not significantly alter the catalytic response of the Pt site, but the stability in acetylene hydrochlorination is markedly affected. Specifically, on NC, coking has been identified as the major reason for catalyst deactivation, which is possibly promoted by N-pyrrolic defects *via* the highly exothermic insertion of acetylene and formation of 7-memberd rings. On the contrary, acetylene chemisorption on O-defects is less favourable, explaining the significantly reduced formation of carbonaceous residues over Pt/AC catalysts. The intrinsic stability of Pt single atoms on this carrier endows them unparalleled durability in acetylene hydrochlorination, ultimately surpassing the space-time-yields of state-of-the-art Au and Ru-based catalysts. This remarkable result in combination with the benign and easily scalable synthesis protocol for Pt SACs as well as the significant price advantage over Au finally re-qualify the previously neglected metal and thereby opens up an alternative direction towards sustainable vinyl chloride production. Going beyond hydrochlorination, our approach to control the reactivity of platinum atoms is generally applicable to other areas and gives perspectives for the tunability of metal species for a wide range of catalytic applications.

Europe PMC Funders Author Manuscripts

Europe PMC Funders Author Manuscripts

Methods

Catalyst synthesis

The N-doped carbon support (NC) was prepared *via* a two-step synthesis, comprising the oxidative polymerisation of aniline and a subsequent carbonisation step.[42] Aniline (50 mmol, Acros, 99.5%) was dissolved in deionised water (40 cm^3, pH 0.4; adjusted by hydrochloric acid, 1.25 M, Sigma Aldrich, >37%), cooled to 277 K, and subsequently added to a precooled solution (277 K) of ammonium persulfate (100 mmol, Acros, 98%) in deionised water (20 cm^3) under vigorous stirring, using a magnetic stirring bar. Subsequently, the polyaniline slurry was kept for 24 h at room temperature without stirring, followed by filtering, and washing with water (*ca.* 0.75 L g^{-1}). The formed polyaniline was dried in static air at 393 K for 12 h and carbonised at 1073 K in N_2 atmosphere for 1 h with a heating rate of 5 K min^{-1}. The obtained N doped carbon was ground and sieved into particles with a size of 0.4-0.6 mm. Commercial activated carbon (Norit ROX 0.8) was immersed in aqua regia at room temperature to remove metal impurities. After filtration and thorough washing with deionised water (2 L g^{-1}), the material was dried in static air at 393 K for 12 h and subsequently ground and sieved into particles with a size of 0.4-0.6 mm. All metal-based catalysts were prepared *via* an incipient wetness impregnation method (nominal metal loading of 1 wt.%). Accordingly, a solution of the respective metal precursor, H_2PtCl_6 (ABCR, 99.9%, 40.0 wt.% Pt) and $HAuCl_4{\cdot}xH_2O$ (ABCR, 99.9%, 49.5 wt.% Au) in water (w, 1.5 cm^3 g^{-1}) or aqua regia (a, 1.5 cm^3 g^{-1}), was added dropwise to the carbon carriers under continuous magnetic stirring for 2 h. Subsequently, all samples were dried at 473 K (static air, 16 h, heating rate = 5 K min^{-1}) prior to thermal activation at higher temperatures, as indicated in the respective sample code (T_{act} = 473-1073 K, 16 h, N_2 for T_{act} > 473 K, heating rate = 5 K min^{-1}), yielding three series of Pt catalysts: (*i*) Pt/NC w T_{act}, (*ii*) Pt/AC-w-T_{act}, and (*iii*) Pt/AC-a T_{act}. The reference gold single-atom catalysts, Au/NC and Au/AC, and the graphene-confined ruthenium-based system (Ru/NC) were obtained *via* thermal activation at 473 K (16 h, static air) and 1073 K (16 h, N_2 atmosphere), respectively, using aqua regia as impregnation solvent.[9,25] The sulphur modified Au-S/AC catalyst (1 wt.% Au) was prepared according to a patented protocol.[43]Accordingly, an aqueous solution of $HAuCl_4{\cdot}xH_2O$ (0.1 cm^3 mg^{-1}) was added to an aqueous solution of ammonium thiosulphate (0.03 cm^3 mg^{-1}, Sigma Aldrich, 98%). The resulting mixture was further diluted (1.5 cm^3 g^{-1}), added dropwise to the AC support under continuous magnetic stirring, and dried (T_{act} = 378 K, 16 h, static air). An overview of all catalysts developed in this study with respective sample codes and synthesis conditions is given in the Supplementary Table 1.

Catalyst characterisation

Inductively coupled plasma-optical emission spectrometry (ICP-OES) was conducted using a Horiba Ultra 2 instrument equipped with photomultiplier tube detection. The solids were dissolved in a 3:1-mixture of HNO_3 and H_2O_2 under sonication until the absence of visible solids. Elemental analysis of C, H, and N was determined by infrared spectroscopy using a LECO TruSpec Micro combustion furnace. Powder X-ray diffraction (XRD) was measured using a PANalytical X'Pert PRO-MPD diffractometer with Cu-Kα radiation (λ = 1.54060 Å). The data was recorded in the 10-70° 2θ range with an angular step size of 0.017° and a counting time of 0.26 s per step. Argon sorption was measured at 77 K in a Micromeritics

Europe PMC Funders Author Manuscripts

Europe PMC Funders Author Manuscripts

3Flex instrument, after evacuation of the samples at 423 K for 12 h. Thermogravimetric analysis (TGA) was performed using a Linseis STA PT1600 system coupled to a Pfeiffer Vacuum Thermo-Star GSD 320 T1 mass spectrometer (MS). TGA of the as-prepared catalysts and after use in acetylene hydrochlorination was carried out in diluted oxygen (20% O_2/Ar, 100 cm^3 min^{-1}), heating the samples (amount fixed to 20 mg) from 298 to 1273 K at 10 K min^{-1} to quantify the amount of coke deposits in the used catalysts. Temperature-programmed desorption of acetylene (C_2H_2-TPD) was performed in a Micromeritics Autochem II 2920 unit equipped with a thermal conductivity detector (TCD) and a Pfeiffer Vacuum OmniStar GSD 320 O MS. The sample (amount fixed to 100 mg) was loaded into a U-shaped quartz micro-reactor, pre-dried in He (T = 473 K, 2 h, F_T = 20 cm^3 min^{-1}, heating rate = 5 K min^{-1}), cooled to 323 K, and subsequently saturated with acetylene (T = 323 K, 20 min, F_T = 10 cm^3 min^{-1}). After purging with He (T = 323 K, 60 min, F_T = 20 cm^3 min^{-1}), the desorption was initiated by increasing the temperature to 473 K using a ramp of 5 K min^{-1}, while monitoring the desorbed C_2H_2 by MS. Scanning transmission electron micrographs (STEM) with a high-angle annular dark-field (HAADF) detector were acquired on a HD2700CS (Hitachi) microscope operated at 200 kV. Samples were prepared by dipping the copper grid supporting a holey carbon foil in a suspension of the solid in ethanol and drying in air. X-ray photoelectron spectra (XPS) were acquired on a Physical Electronics Quantum 2000 instrument using monochromatic Al-Kα radiation, generated from an electron beam operated at 15 kV, and equipped with a hemispherical capacitor electron-energy analyser. The samples were analysed at an electron take-off angle of 45° and a constant analyser pass energy of 46.95 eV with a spectra resolution step width of 0.2 eV. The spectrometer was calibrated for the Au 4$f_{7/2}$ signal at 84.0 ± 0.1 eV. The elemental concentrations, given in Table 1, were quantified based on the measured photoelectron peak areas (C 1s, N 1s, O 1s, Cl 2p), using PHI-MultiPak software and the built-in relative sensitivity factors, which are corrected for the system transmission function. The Pt 4f and N 1s spectra were fitted by mixed Gaussian-Lorentzian component profiles after Shirley background subtraction (68-81 eV for Pt 4f spectra and 309-405 eV for N 1s respectively). The selected peak positions of the $Pt^{7/2}$ doublet peak are based on literature reported data (71.2±0.1 eV for Pt(0), 72.4±0.1 eV for Pt(II), and 73.6±0.1 eV for Pt in a higher oxidation state, tentatively assigned to Pt(IV).[37,40] The areal ratio of the $Pt^{7/2}$ to $Pt^{5/2}$ was fixed to 4:3 and the peak separation to 3.33 eV. The full width at half maximum (FWHM) of the two $Pt^{7/2}$ and $Pt^{5/2}$ doublet peaks has been locked to obtain the same values for each single component. However, for different components the FWHM was not restricted, resulting in small variations in the FWHM (±0.25) for different doublet-peaks. These small variations occur due to locally differing environments (*i.e.*, variations in the chemical bonding with the second or third neighbouring atom and local variations in the Fermi level for compounds having a band gap). The selected peak positions for the four different nitrogen species have been fixed to 398.4 eV (N6), 400.4 eV (N5), 401.1 eV (N3), and 403.0 eV (N0) with an error of ±0.1 eV.[42] The FWHM was not restricted, resulting in small variations (±0.25) for different peaks. The detailed fitting parameters, reported in literature and used in this work, are given in Supplementary Tables 2,3. X-ray absorption fine structure (XAFS) measurements at the Pt L_2 and L_3-edge were carried out at the SuperXAS beamline of the Swiss Light Source. The incident photon beam provided by a 2.9 T superbend magnet was selected by a Si(111) channel-cut Quick-EXAFS monochromator.

Europe PMC Funders Author Manuscripts

Europe PMC Funders Author Manuscripts

The rejection of higher harmonics and focusing were achieved with rhodium-coated collimating and toroidal mirrors, respectively, at 2.5 mrad. The beamline was calibrated using Pt foil. The area of sample illuminated by the X-ray beam was 0.5 mm×0.2 mm. The Pt catalysts (300 mg) were finely ground, mixed homogeneously with five parts of cellulose, and pressed into 13 mm diameter pellets. Commercial H_2PtCl_6 (ABCR, 99.9%), $PtCl_2$ (ACROS, 99.9%), PtO_2 (ABCR, 99.95%), and $Pt(NH_3)_4(NO_3)_2$ (Sigma-Aldrich, 99.995%) were used as references. All spectra were recorded in transmission mode at room temperature. The extended X-ray absorption fine structure (EXAFS) spectra were acquired with a 1 Hz frequency (0.5 s per spectrum) and then averaged over 10 min. The X-ray absorption near-edge structure (XANES) spectra were calibrated by measuring Pt foil simultaneously with each sample. The EXAFS spectra were analysed using the Demeter software package.[44] The background signal before the Pt L_3-edge was subtracted using a linear function (fitting range between –150 and –60 eV). The post edge signal was normalised to the step of one using a Victoreen function in the region between 150 and 1300 eV after the edge. The background signal before the Pt L_2-edge was subtracted using a linear function (fitting range between –150 and –60 eV). The post edge signal was normalised to the step of one using a Victoreen function in the region between 100 and 600 eV after the edge. We fitted the k^3 weighted Fourier transformed signal and determined an amplitude reduction factor (S_0^2) of 0.83 from the EXAFS fit of the Pt metal foil. All EXAFS spectra were fitted for the first coordination shell in the k-range of 3.2-9.5 and 3.1-9.9 $Å^{-1}$, for L_3 and L_2 edges, respectively and R-range of 1.1-2.85 Å. To fit the Pt–Pt, Pt–Cl, and Pt–N(O) scattering paths, Pt foil, H_2PtCl_6, and PtO_2 were used as the references (Supplementary Figure 6).

Catalyst testing

Steady-state hydrochlorination of acetylene was studied at atmospheric pressure in a continuous-flow fixed-bed micro-reactor (Supplementary Figure 20).[9] The gases C_2H_2 (PanGas, purity 2.6), HCl (Air Liquide, purity 2.8, anhydrous), Ar (PanGas, purity 5.0, internal standard), and He (PanGas, purity 5.0, carrier gas), were fed using digital mass-flow controllers (Bronkhorst) to the mixing unit, equipped with a pressure indicator. A quartz micro-reactor of 10 mm inner diameter was loaded with the catalyst (W_{cat} = 0.1 g in initial catalytic activity tests and 0.25 g in stability tests, particle size 0.4-0.6 mm) and placed in a homemade electrical oven. A K type thermocouple fixed in a coaxial quartz thermowell with the tip positioned in the centre of the catalyst bed was used to control the temperature during the reaction. Prior to testing, the catalyst was heated in a He flow to the desired temperature (T_{bed} = 423 493 K) and allowed to stabilise for at least 30 min before the reaction mixture (40 vol.% C_2H_2, 44 vol.% HCl, and 16 vol.% Ar; in the case of Ru/NC[25] additional 0.5 vol.% O_2) was fed at a total volumetric flow of F_T = 15 cm^3 STP min^{-1}. Carbon containing compounds (C_2H_2 and C_2H_3Cl) and Ar were quantified on line *via* a gas chromatograph equipped with a GS Carbon PLOT column coupled to a mass spectrometer (GC-MS, Agilent, GC 7890B, Agilent MSD 5977A). Since vinyl chloride (VCM) was the only product detected in all our tests, the catalytic activity is presented as the yield of VCM, Y(VCM), calculated according to Equation 1,

Europe PMC Funders Author Manuscripts

Europe PMC Funders Author Manuscripts

$$Y(\mathrm{VCM}) = \frac{n_{\mathrm{VCM}}^{\mathrm{outlet}}}{n_{\mathrm{C_2H_2}}^{\mathrm{inlet}}} \cdot 100 \tag{1}$$

where $n_{\mathrm{VCM}}^{\mathrm{outlet}}$ and $n_{\mathrm{C_2H_2}}^{\mathrm{inlet}}$ denote the respective molar flows of VCM and C_2H_2 at the reactor outlet and inlet. The turnover frequency (*TOF*) and the space-time yield (STY) of VCM were determined according to Equations 2 and 3,

$$TOF = \frac{n_{\mathrm{C_2H_2}}^{\mathrm{inlet}} - n_{\mathrm{C_2H_2}}^{\mathrm{outlet}}}{n_{\mathrm{Pt}}} \tag{2}$$

$$STY(\mathrm{VCM}) = \frac{n_{\mathrm{VCM}}^{\mathrm{outlet}}}{W_{\mathrm{cat}}} \cdot M(\mathrm{VCM}) \tag{3}$$

The error of the carbon balance, ε_{C}, determined using Equation 4, was less than 5% in all experiments, *i.e.*, the carbon mass balance was closed at ≥ 95%.

$$\varepsilon_{\mathrm{C}} = \frac{n_{\mathrm{C_2H_2}}^{\mathrm{inlet}} - \left(n_{\mathrm{C_2H_2}}^{\mathrm{outlet}} + n_{\mathrm{VCM}}^{\mathrm{outlet}}\right)}{n_{\mathrm{C_2H_2}}^{\mathrm{inlet}}} \cdot 100 \tag{4}$$

After the tests, the reactor was quenched to room temperature in He flow and the catalyst was retrieved for further characterisation. All catalytic data points were determined as an average of at least two measurements. The evaluation of the dimensionless moduli based on the criteria of Carberry, Mears, and Weisz–Prater confirmed that all the catalytic tests were performed in the absence of mass and heat transfer limitations (see Supplementary Table 8 and SupplementaryDiscussion). The deactivation constants, k_{D}, were derived *via* a simple linear regression of the initial time-on-stream (*tos*) performances of selected platinum and gold-based catalysts (linear regime). For clarity, the considered data ranges are indicated by the respective trend lines in Supplementary Figure 10.

Computational methods

Spin polarised density functional theory (DFT) calculations were performed using the Vienna *Ab initio* Simulation Package (VASP) code.[45,46] The functional of choice was Perdew-Becke-Ernzerhof (PBE)[47] with dispersion contributions introduced through the D3 approach.[48,49] While non-valent electrons were described by projector augmented-waves (PAW)[50,51] the valence monoelectronic states were expanded as plane waves with maximum kinetic energy of 450 eV. Graphitic carbon slabs were modelled using a 6×6 supercell with three layers of thickness. The metal surfaces were modelled using a 4×4 supercell in the (111) orientation. For all systems the top two layers of the slab were allowed to relax and the slabs were separated by 12 Å of vacuum. The k-points sampling was a Γ–centered 3×3×1 grid (~0.3 $Å^{-1}$). A dipole correction was employed along the z-direction normal to the slab faces.[52] The molecules were placed in a cubic box of 15 Å sides. In all cases the optimisation thresholds were 10^{-5} and 10^{-4} eV for electronic and ionic relaxations, respectively (VASP recommended and tested settings for graphitic materials). Transition

states were located following the climbing image nudged elastic band procedure (CI-NEB).[53] Transition states were confirmed by diagonalising the numerical Hessian matrix obtained by ±0.02 Å displacements. Simulated EXAFS spectra were generated using FEFF8[44] and post-processed with Athena.[54] All structures presented in this work can be retrieved from the ioChem-BD database.[55,56]

Supplementary Material

Refer to Web version on PubMed Central for supplementary material.

Acknowledgements

This work was supported by ETH research grant (ETH-40 17-1) and the Swiss National Science Foundation (project no. 200021-169679). E.F. thanks MINECO La Caixa Severo Ochoa for a predoctoral grant through Severo Ochoa Excellence Accreditation 2014-2018 (SEV 2013 0319). BSC-RES for providing generous computational resources. The Scientific Centre for Optical and Electron Microscopy (ScopeM) at ETH Zurich is acknowledged for the use of their facilities and the Micromeritics Grant Program is thanked for the award of the 3Flex instrument.

References

1. Zhang Z, et al. Thermally stable single atom Pt/m-Al_2O_3 for selective hydrogenation and CO oxidation. Nat Commun. 2017; 8
2. Zhang L, et al. Single-atom catalyst: a rising star for green synthesis of fine chemicals. Natl Sci Rev. 2018; 5:653–672.
3. Zhang J, Alexandrova AN. The golden crown: a single Au atom that boosts the CO oxidation catalyzed by a palladium cluster on titania surfaces. J Phys Chem Lett. 2013; 4:2250–2255.
4. Yang M, Flytzani-Stephanopoulos M. Design of single-atom metal catalysts on various supports for the low-temperature water-gas shift reaction. Catal Today. 2017; 298:216–225.
5. Zhang B, et al. Atomically dispersed Pt_1-polyoxometalate catalysts: how does metal-support interaction affect stability and hydrogenation activity? J Am Chem Soc. 2019; 141:8185–8197. [PubMed: 31030515]
6. Wang A, Li J, Zhang T. Heterogeneous single-atom catalysis. Nat Rev Chem. 2018; 2:65–81.
7. Li M, et al. Single-atom tailoring of platinum nanocatalysts for high-performance multifunctional electrocatalysis. Nat Catal. 2019; 2:495–503.
8. Xu H, Cheng D, Cao D, Zeng XC. A universal principle for a rational design of single-atom electrocatalysts. Nat Catal. 2018; 1:339–348.
9. Kaiser SK, et al. Controlling the speciation and reactivity of carbon-supported gold nanostructures for catalysed acetylene hydrochlorination. Chem Sci. 2019; 10:359–369. [PubMed: 30746085]
10. Lin R, et al. Design of single gold atoms on nitrogen-doped carbon for molecular recognition in alkyne semi-hydrogenation. Angew Chem Int Ed. 2019; 58:504–509.
11. Yin XP, et al. Engineering the coordination environment of single-atom platinum anchored on graphdiyne for optimizing electrocatalytic hydrogen evolution. Angew Chem Int Ed. 2018; 57:9382–9386.
12. Liu W, et al. Discriminating catalytically active FeN_x species of atomically dispersed Fe-N-C catalyst for selective oxidation of the C-H bond. J Am Chem Soc. 2017; 139:10790–10798. [PubMed: 28745500]
13. Wang X, et al. Regulation of coordination number over single co sites: triggering the efficient electroreduction of CO_2. Angew Chem Int Ed. 2018; 57:1944–1948.
14. Mitchell S, Vorobyeva E, Pérez-Ramírez J. The multifaceted reactivity of single-atom heterogeneous catalysts. Angew Chem Int Ed. 2018; 57:15316–15329.
15. Lin R, Amrute AP, Pérez-Ramírez J. Halogen-mediated conversion of hydrocarbons to commodities. Chem Rev. 2017; 117:4182–4247. [PubMed: 28150944]

Europe PMC Funders Author Manuscripts
Europe PMC Funders Author Manuscripts

Europe PMC Funders Author Manuscripts

Europe PMC Funders Author Manuscripts

16. Zhu M, et al. Development of a heterogeneous non-mercury catalyst for acetylene hydrochlorination. ACS Catal. 2015; 5:5306–5316.
17. Zhong J, Xu Y, Liu Z. Heterogeneous non-mercury catalysts for acetylene hydrochlorination: progress, challenges, and opportunities. Green Chem. 2018; 20:2412–2427.
18. United Nations Environment Programme. [Accessed August 2019] Minamata Convention on Mercury. 2013. www.mercuryconvention.org/
19. Malta G, Freakley SJ, Kondrat SA, Hutchings GJ. Acetylene hydrochlorination using Au/carbon: a journey towards single site catalysis. Chem Commun. 2017; 53:11733–11746.
20. Johnston P, Carthey N, Hutchings GJ. Discovery, development, and commercialization of gold catalysts for acetylene hydrochlorination. J Am Chem Soc. 2015; 137:14548–14557. [PubMed: 26529366]
21. Shang S, et al. Highly efficient Ru@IL/AC to substitute mercuric catalyst for acetylene hydrochlorination. ACS Catal. 2017; 7:3510–3520.
22. Malta G, et al. Identification of single-site gold catalysis in acetylene hydrochlorination. Science. 2017; 355:1399–1403. [PubMed: 28360324]
23. Malta G, et al. Deactivation of a single-site gold-on-carbon acetylene hydrochlorination catalyst: an X-ray absorption and inelastic neutron scattering study. ACS Catal. 2018; 8:8493–8505.
24. Ye L, et al. Self-regeneration of Au/CeO_2 based catalysts with enhanced activity and ultra-stability for acetylene hydrochlorination. Nat Commun. 2019; 10:914. [PubMed: 30796236]
25. Kaiser SK, et al. Preserved in a shell: the high performance of graphene-confined ruthenium nanoparticles in acetylene hydrochlorination. Angew Chem Int Ed. 2019; 58:12297–12304.
26. Zhou K, et al. A low content Au-based catalyst for hydrochlorination of C_2H_2 and its industrial scale-up for future PVC processes. Green Chem. 2015; 17:356–364.
27. Conte M, et al. Hydrochlorination of acetylene using supported bimetallic Au-based catalysts. J Catal. 2008; 257:190–198.
28. London Bullion Market Association (LBMA). [Accessed September 2019] Precious metals prices. http://www.lbma.org.uk/precious-metal-prices
29. Figueroba A, Kovács G, Bruix A, Neyman KM. Towards stable single-atom catalysts: strong binding of atomically dispersed transition metals on the surface of nanostructured ceria. Catal Sci Technol. 2016; 6:6806–6813.
30. Pierre D, Deng W, Flytzani-Stephanopoulos M. The importance of strongly bound Pt–CeO_x species for the water-gas shift reaction: catalyst activity and stability evaluation. Top Catal. 2007; 46:363–373.
31. O'Connor NJ, Jonayat ASM, Janik MJ, Senftle TP. Interaction trends between single metal atoms and oxide supports identified with density functional theory and statistical learning. Nat Catal. 2018; 1:531–539.
32. Daelman N, Capdevila-Cortada M, López N. Dynamic charge and oxidation state of Pt/CeO_2 single-atom catalysts. Nat Mater. 2019
33. Leyva-Pérez A, Corma A. Similarities and differences between the "relativistic" triad gold, platinum, and mercury in catalysis. Angew Chem Int Ed. 2012; 51:614–635.
34. Hu J, et al. Confining noble metal (Pd, Au, Pt) nanoparticles in surfactant ionic liquids: active non-mercury catalysts for hydrochlorination of acetylene. ACS Catal. 2015; 5:6724–6731.
35. Mitchenko SA, Krasnyakova TV, Mitchenko RS, Korduban AN. Acetylene catalytic hydrochlorination over powder catalyst prepared by pre-milling of K_2PtCl_4 salt. J Mol Catal A Chem. 2007; 275:101–108.
36. Yang L, et al. Metal nanoparticles in ionic liquid-cosolvent biphasic systems as active catalysts for acetylene hydrochlorination. AIChE J. 2018; 64:2536–2544.
37. Yang M, et al. A common single-site Pt(II)-$O(OH)_x$- species stabilized by sodium on "active" and "inert" supports catalyzes the water-gas shift reaction. J Am Chem Soc. 2015; 137:3470–3473. [PubMed: 25746682]
38. Spieker WA, Liu J, Miller JT, Regalbuto JR. An EXAFS study of the co-ordination chemistry of hydrogen hexachloroplatinate(IV) 1. Speciation in aqueous solution. Appl Catal A. 2002; 232:219–235.

Europe PMC Funders Author Manuscripts

Europe PMC Funders Author Manuscripts

39. Fraga MA, et al. Properties of carbon-supported platinum catalysts: Role of carbon surface sites. J Catal. 2002; 209:355–364.
40. Chen Z, et al. Stabilization of single metal atoms on graphitic carbon nitride. Adv Funct Mater. 2017; 27
41. Lei Y, et al. Effect of particle size and adsorbates on the L_3, L_2 and L_1 X-ray absorption near edge structure of supported Pt nanoparticles. Top Catal. 2011; 54:334–348.
42. Lin R, Kaiser SK, Hauert R, Pérez-Ramírez J. Descriptors for high-performance nitrogen-doped carbon catalysts in acetylene hydrochlorination. ACS Catal. 2018; 8:1114–1121.
43. Bishop, PT; Carthey, NA; Peter, J. Catalyst comprising gold and a sulphur containing ligand on a support and method for its preparation. Pat WO 2013/008004A3. 2013.
44. Newville M. IFEFFIT: Interactive XAFS analysis and FEFF fitting. J Synchrotron Rad. 2001; 8:322–324.
45. Kresse G, Furthmüller J. Efficiency of *ab initio* total energy calculations for metals and semiconductors using a plane-wave basis set. Comp Mater Sci. 1996; 6:15–50.
46. Kresse G, Furthmüller J. Efficient iterative schemes for *ab initio* total-energy calculations using a plane-wave basis set. Phys Rev B. 1996; 54:11169–11186.
47. Perdew JP, Burke K, Ernzerhof M. Generalized gradient approximation made simple. Phys Rev Lett. 1996; 77:3865–3868. [PubMed: 10062328]
48. Grimme S. Semiempirical GGA-type density functional constructed with a long-range dispersion correction. J Comput Chem. 2006; 27:1787–1799. [PubMed: 16955487]
49. Grimme S, Antony J, Ehrlich S, Krieg H. A consistent and accurate *ab initio* parametrization of density functional dispersion correction (DFT-D) for the 94 elements H-Pu. J Chem Phys. 2010; 132
50. Blöchl PE. Projector augmented-wave method. Phys Rev B. 1994; 50:17953–17979.
51. Kresse G, Joubert D. From ultrasoft pseudopotentials to the projector augmented-wave method. Phys Rev B. 1999; 59:1758–1775.
52. Makov G, Payne MC. Periodic boundary conditions in *ab initio* calculations. Phys Rev B. 1995; 51:4014–4022.
53. Henkelman G, Jónsson H. Improved tangent estimate in the nudged elastic band method for finding minimum energy paths and saddle points. J Chem Phys. 2000; 113:9978–9985.
54. Ravel B, Newville M. ATHENA, ARTEMIS, HEPHAESTUS: Data analysis for X-ray absorption spectroscopy using IFEFFIT. J Synchrotron Radiat. 2005; 12:537–541. [PubMed: 15968136]
55. Álvarez-Moreno M, et al. Managing the computational chemistry big data problem: the ioChem-BD platform. J Chem Inf Model. 2015; 55:95–103. [PubMed: 25469626]
56. Fako E. ioChem-BD Collection.

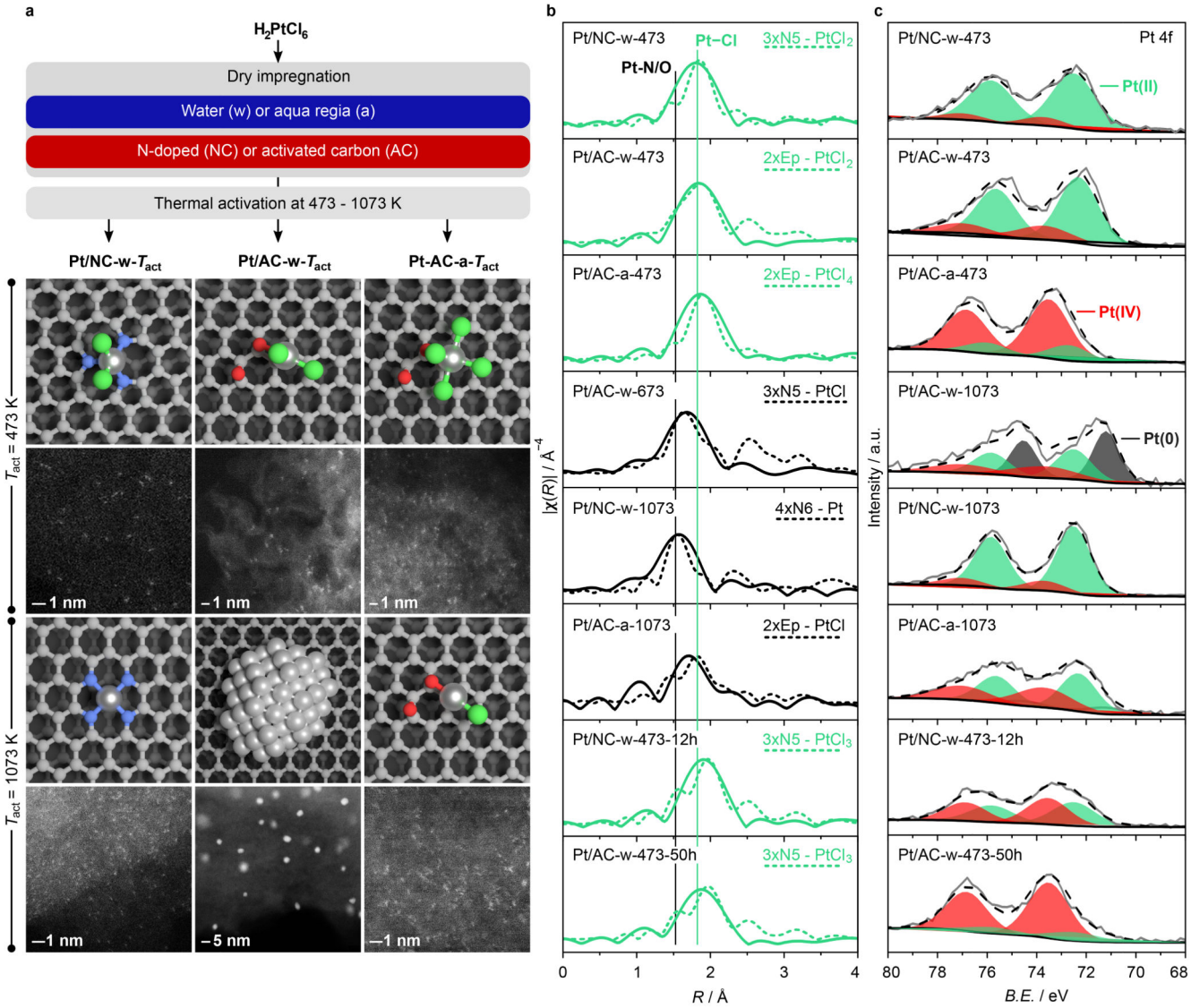

Figure 1. Synthesis and characterisation of carbon-supported Pt catalysts.

(**a**) Synthetic steps involved in the preparation of nitrogen-doped carbon (NC) and activated carbon (AC)-supported platinum nanostructures, accompanied by STEM images and structural representations of selected samples. Colour code: C – grey, N – blue, O – red, H – white, Pt – metallic grey, Cl – green. (**b**) Pt 4*f* XPS and (**c**) Pt L_3 EXAFS spectra of selected catalysts. Dashed black lines in (**b**) show the results of fitting the raw data (solid grey lines). Dotted lines in (**c**) show the L_3 EXAFS simulated DFT data. The vertical lines indicating the Pt−Cl and Pt−O/N peaks are derived from respective reference materials (Supplementary Figure 6). The detailed fitting data is given in Supplementary Figures 7,8).

Europe PMC Funders Author Manuscripts
Europe PMC Funders Author Manuscripts

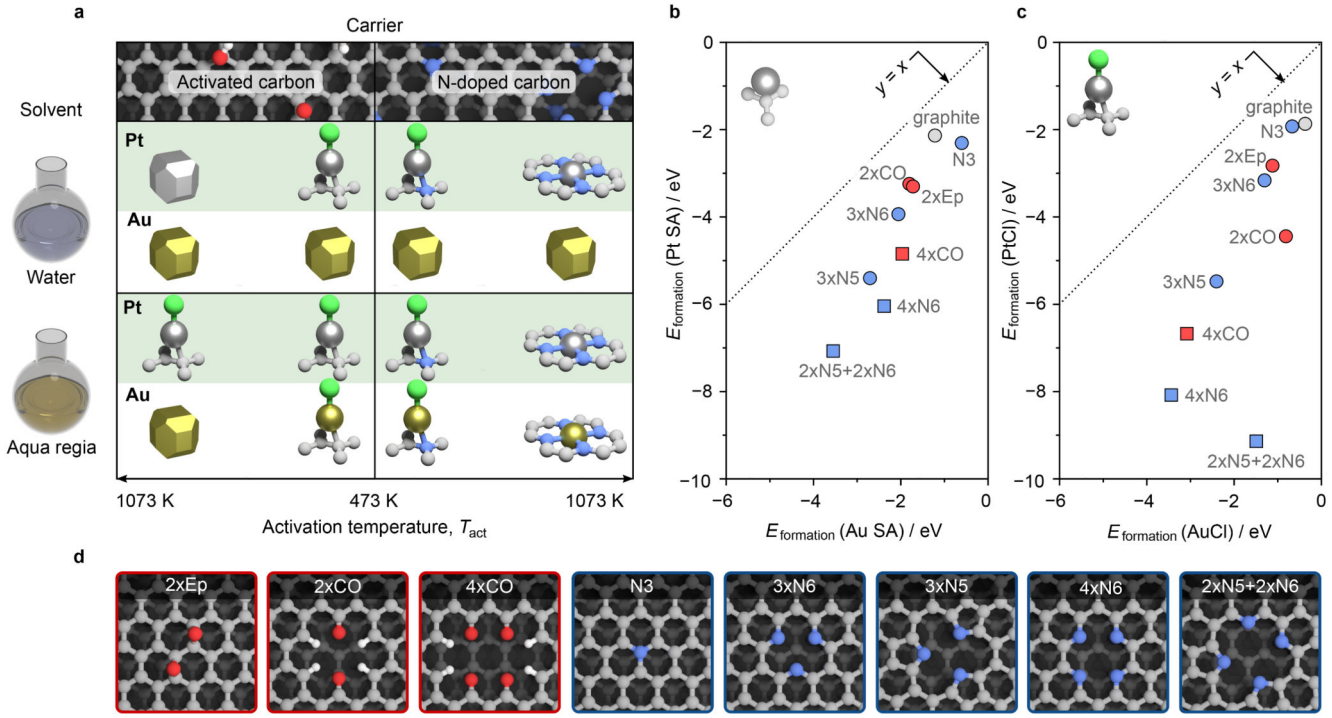

Figure 2. Stability of Pt and Au single atoms on carbon carriers.

(**a**) Combinations of synthesis parameters (*i.e*, carrier, impregnation solvent, activation temperature) that yield gold and platinum single atoms or nanoparticles, respectively, showing the synthetic simplicity of preparing carbon-supported Pt single-atom catalysts and their generally higher thermal stability compared to their gold-based analogues. (**b**, **c)** Correlations of formation energies for the Pt and Au single atom (**b**) and metal chloride species (**c**) computed as the difference in electronic energy of an empty defect and an isolated M/MCl (M = Au, Pt), *versus* the formed SA/MCl motif. (**d**) Nomenclature chart of the subset of N- and O-defects described in (**b**, **c**). The energies are defined as: $E_{formation}$(M SA) = E (def.–M SA) – E (def.) –E (isolated M atom); $E_{formation}$(MCl) = E (def.–MCl) – E (def.) –E (isolated MCl); M = Pt, Au; E (def.–M SA) – energy of formed SA species on defect; E (def.–MCl) – energy of formed MCl species on defect; E (def.) – energy of vacant defect. Colour code: C – grey, N – blue, O – red, H – white, Pt – metallic grey, Au – metallic yellow, Cl – green.

Europe PMC Funders Author Manuscripts
Europe PMC Funders Author Manuscripts

Europe PMC Funders Author Manuscripts

Europe PMC Funders Author Manuscripts

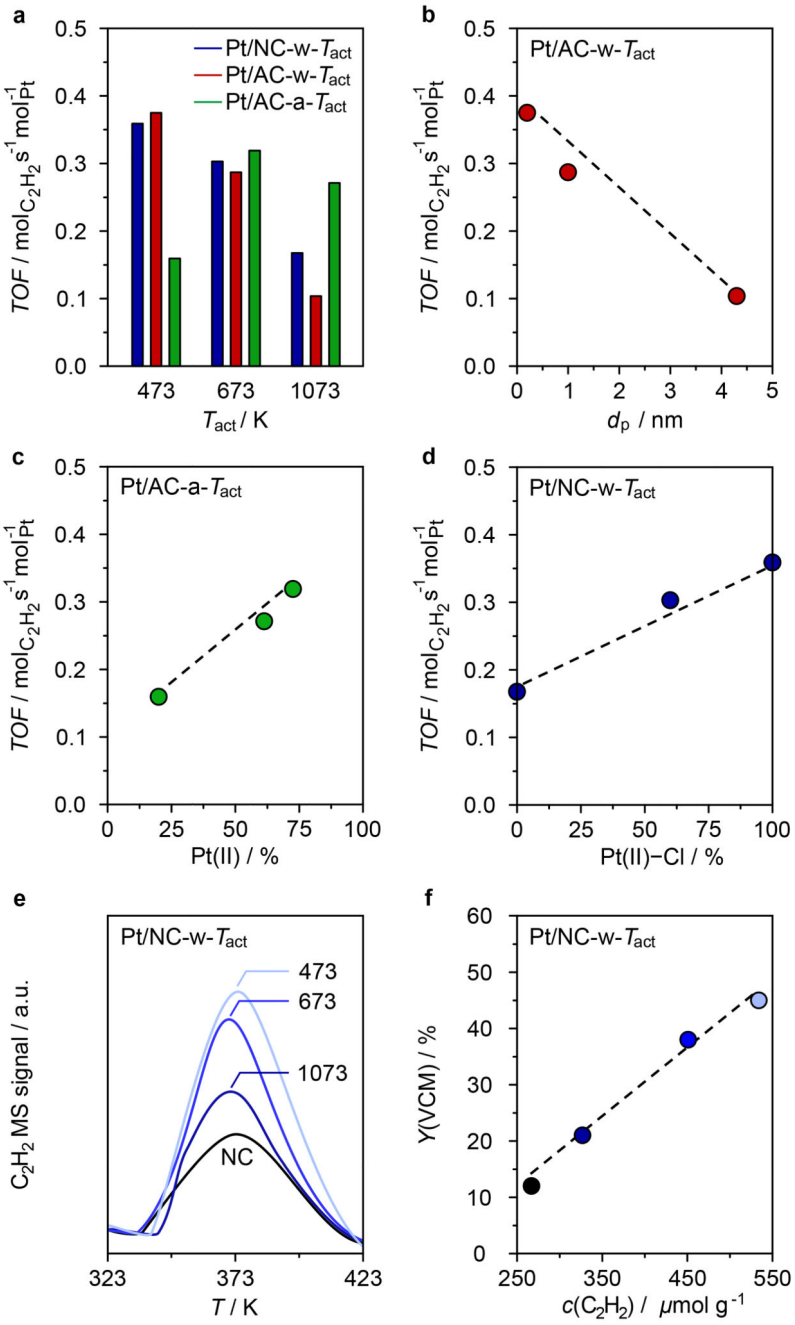

Figure 3. Activity descriptors for Pt catalysts.

Initial activity in acetylene hydrochlorination, expressed as the turnover frequency (*TOF*) or the yield of vinyl chloride monomer, *Y*(VCM), of nanostructured Pt catalysts, as a function of (**a**) the activation temperature applied in the synthesis, (**b**) the mean metal particle size, (**c**) the metal oxidation state of Pt single atoms, and (**d**) the coordination environment of Pt single atoms. (**e**) Acetylene evolution curves obtained from TPD-MS analysis of selected Pt single-atom catalysts, indicating that the coordination environment of Pt(II) single atoms

affects the C_2H_2 adsorption capacity. (**f**) Initial activity as a function of the acetylene adsorption capacity of platinum single-atom catalysts.

Europe PMC Funders Author Manuscripts

Europe PMC Funders Author Manuscripts

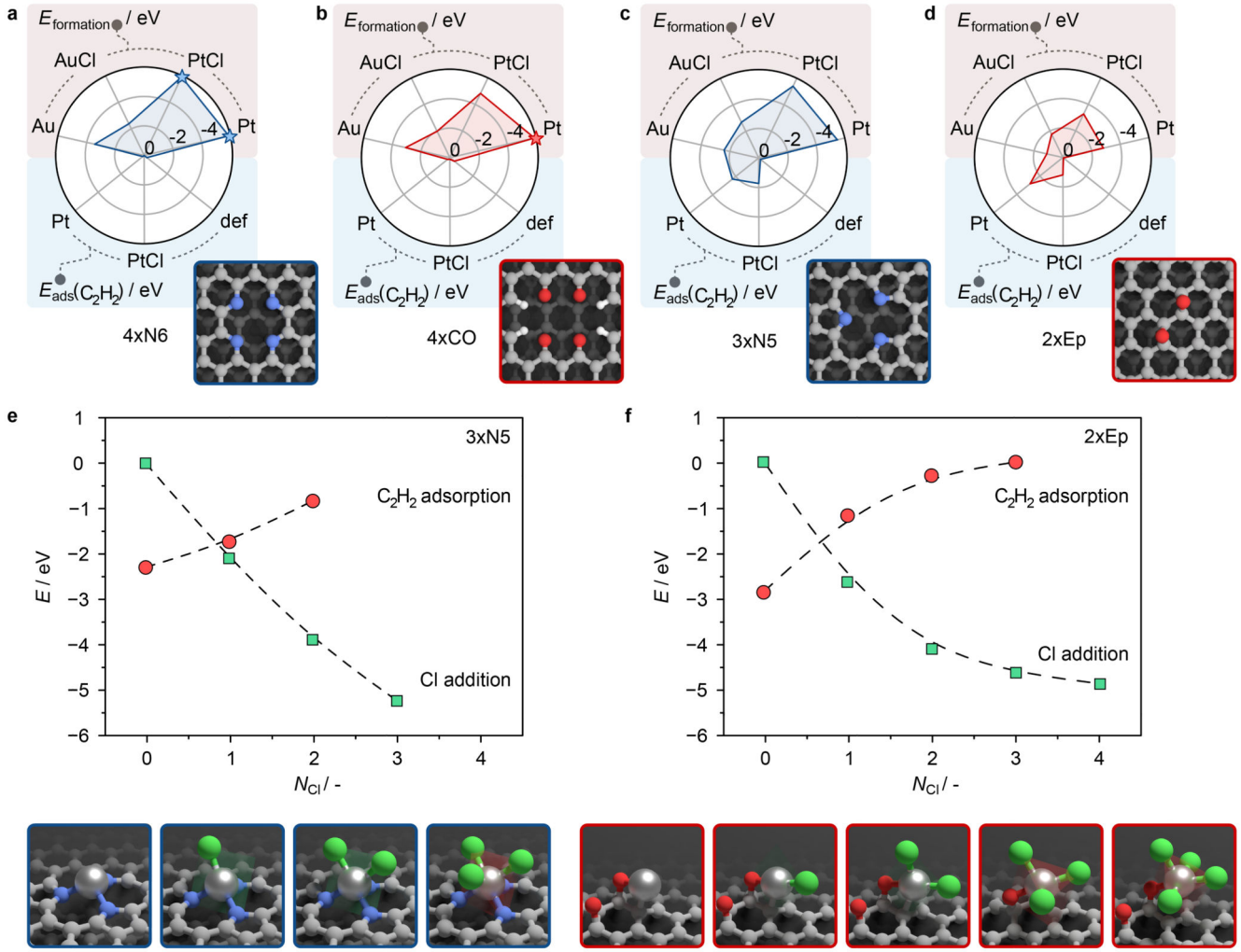

Figure 4. Relationship between the stability of the single-atom species and their ability to adsorb and activate acetylene.

(**a-d**) Radar plots of the interactions with the scaffold and M/MCl (M = Au, Pt), and adsorption of acetylene over Pt and PtCl supported species and the corresponding empty defect (def). (**a**, **b**) Square planar configurations in the basal plane (values marked with a star (★/★) exceed the scale of the plot and are –6.06/–8.08 eV for 4×N6 (PtCl/Pt) and –6.67 eV for Pt at 4×CO). (**c**, **d**) Configurations that allow for the coordination of multiple ligands from the gas phase. (**e**, **f**) Effect of the addition of Cl into the coordination sphere of a SA species on its stability relative to the energy of PtCl (green), and the ability to adsorb acetylene (red). The energies are defined as: **a-d** in Figure 2.; $E_{ads}(C_2H_2) = E(\text{def.–PtCl}_N\text{–}C_2H_2) - E(\text{def.–PtCl}_N) - E(\text{isolated } C_2H_2)$; $E(\text{Cl addition}) = E(\text{def.–PtCl}_N) - E(\text{def.–Pt}) - N/2\, E(\text{isolated } Cl_2)$; $N \in \{0, 1, 2, 3, 4\}$. Colour code: C – grey, N – blue, O – red, H – white, Pt – metallic grey, Cl – green.

Europe PMC Funders Author Manuscripts
Europe PMC Funders Author Manuscripts

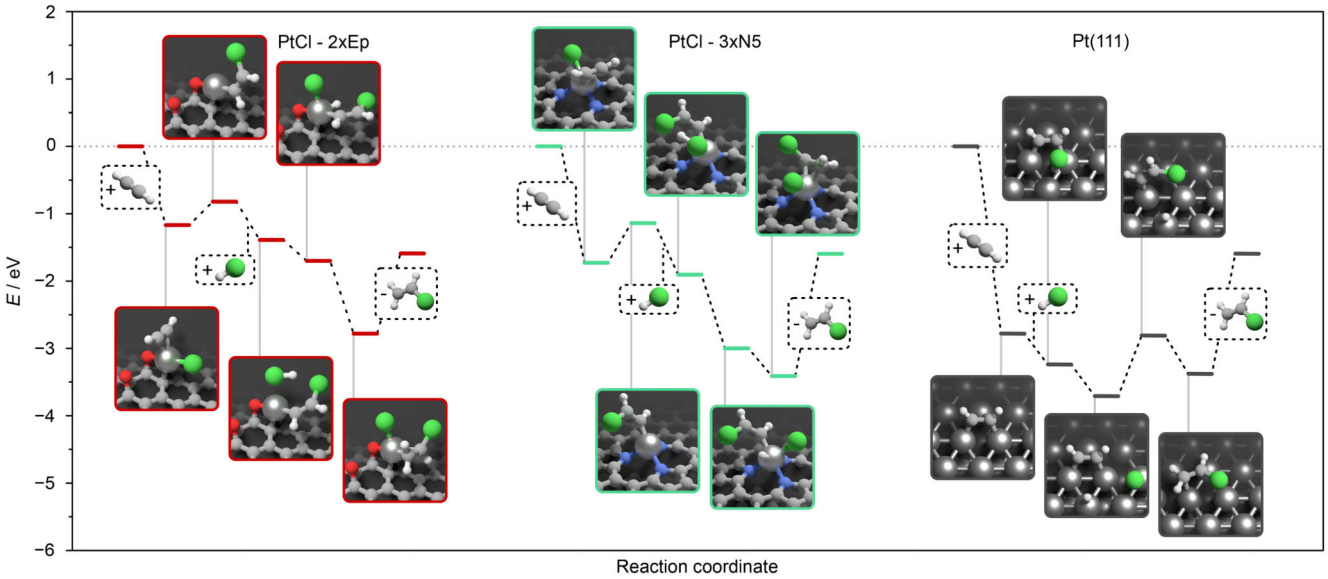

Figure 5. Reaction pathway for acetylene hydrochlorination over distinct Pt sites.

Mechanism over PtCl single-atom species supported on a di-epoxide (2×Ep) defect of the AC support (red) and a tri-pyrrolic (3×N5) defect of the NC support (green) as well as over the Pt(111) surface (dark grey). The energies are defined as: $E = E_{\text{intermediate}}(\text{def.–PtCl–}(C_2H_2)_n\text{–HCl}_m) - E\,(\text{def.–PtCl}) - n\,E\,(\text{isolated } C_2H_2) - m\,E\,(\text{isolated HCl})$; where E – the energy of the intermediate *versus* the reference state (active site, isolated C_2H_2 and HCl molecules); $E_{\text{intermediate}}(\text{def.–PtCl–}(C_2H_2)_n\text{–HCl}_m)$ – electronic energy of the relaxed intermediate (structure illustrated in box). Colour code: C – grey, N – blue, O – red, H – white, Pt – metallic grey, Cl – green.

Europe PMC Funders Author Manuscripts
Europe PMC Funders Author Manuscripts

Europe PMC Funders Author Manuscripts

Europe PMC Funders Author Manuscripts

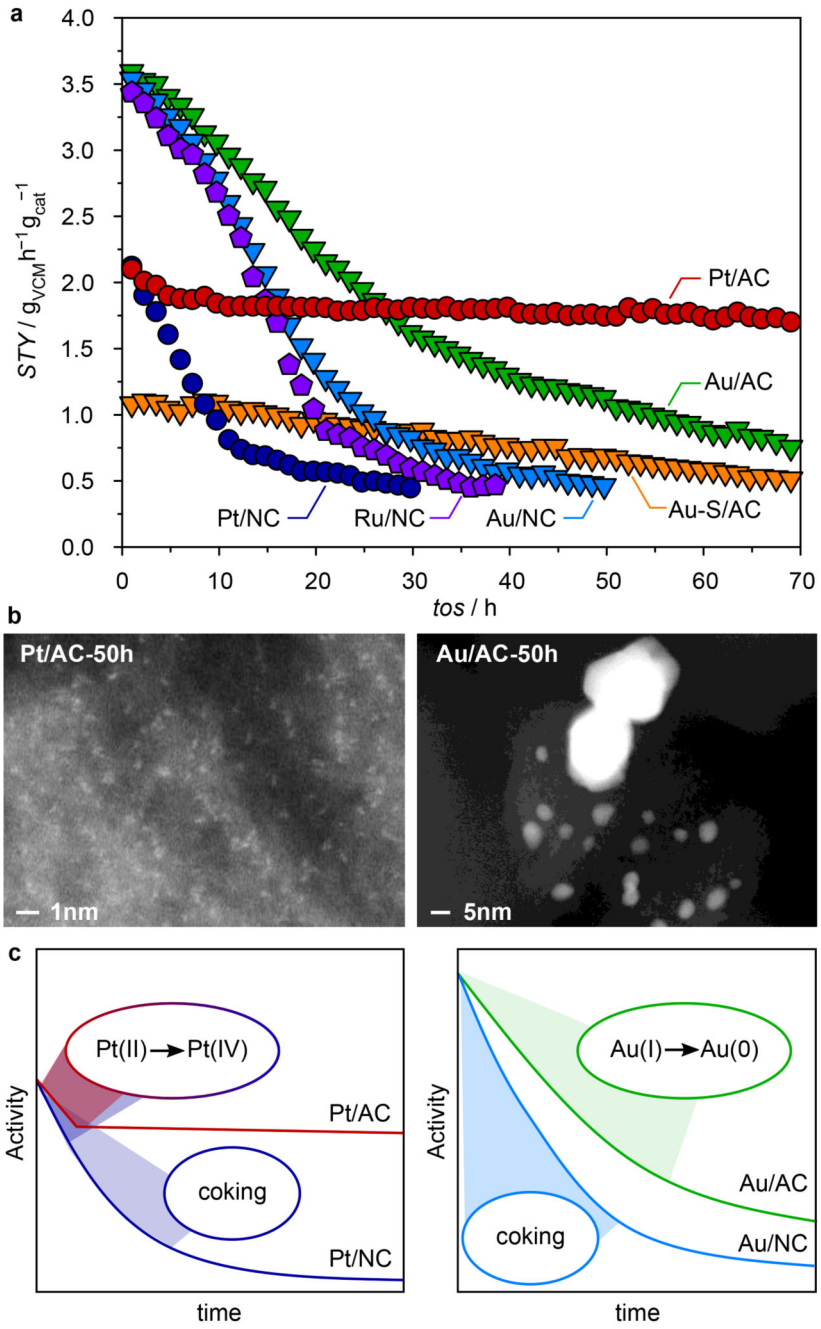

Figure 6. Catalyst stability and deactivation.

(**a**) Time-on-stream (*tos*) performance under accelerated deactivation conditions of selected platinum single-atom catalysts in direct comparison to state-of-the-art ruthenium and gold-based catalysts, Pt/AC w 473, Pt/NC-w-473, Au/AC-a-473,[9] Au/NC-a-473,[9] Ru/NC-a-1073,[25] and $(NH_4)_2Au(S_2O_3)_3$/AC[20,41] (for simplicity denoted as Pt/AC, Pt/NC, Au/AC, Au/NC, Ru/NC, and Au-S/AC, respectively), expressed as space-time-yields (*STY*). (**b**), STEM images of the AC-supported catalysts after use in acetylene hydrochlorination for 50 h, visualising preserved atomic dispersion of Pt and Au particle agglomeration, respectively.

(**c**), Comparison of the major deactivation paths identified for Pt and Au single atoms hosted on AC and NC.

Europe PMC Funders Author Manuscripts

Europe PMC Funders Author Manuscripts

Europe PMC Funders Author Manuscripts

Europe PMC Funders Author Manuscripts

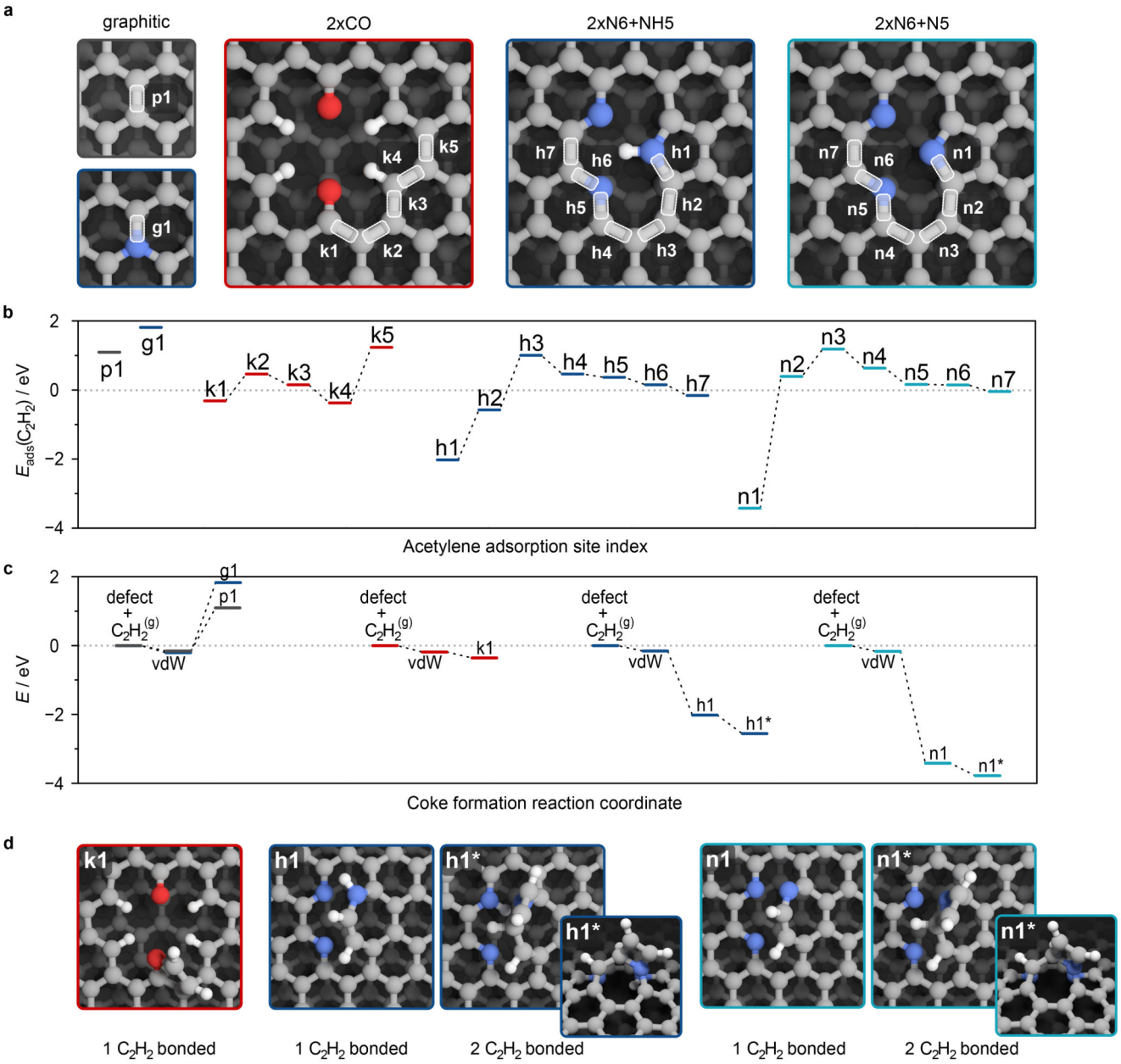

Figure 7. Coke formation over the AC and NC carrier.

C_2H_2 is adsorbed from the gas phase on the edges of defect sites (**a**) that include pristine graphite (p1), graphitic nitrogen (g1), keto group (2×CO, k1-k5), and pyrrolic/pyridinic-N atoms (2×N6+NH5, h1-h7; 2×N6+N5. n1-n7). In all structures, C_2H_2 is chemically bound to the graphitic basal plane (van der Waals (vdW) adsorption is shown in Supplementary Figures 13, 14), and the energy changes represented in (**b**). Coke formation is described as a reaction pathway (**c**) where an acetylene molecule is adsorbed on the top of the defect by vdW forces and chemically bound (g1, p1, k1, h1 and n1). A second C_2H_2 molecule is then chemically bound to h1 and n1 yielding h1* and n1*. The energies are defined as: $E_{ads.}$

$(C_2H_2) = E_{intermediate}(def.–(C_2H_2)_n) – E\,(def.) – n\,E\,(isolated\ C_2H_2)$; Colour code: C – grey, N – blue, O – red, H – white.

Europe PMC Funders Author Manuscripts

Europe PMC Funders Author Manuscripts

Europe PMC Funders Author Manuscripts

Europe PMC Funders Author Manuscripts

Table 1

Metal content and surface atomic concentrations of selected catalysts.

Catalyst	Pt[a]/ wt.%	Pt[b]/ at.%	C[b]/ at.%	N[b]/ at.%	O[b]/ at.%	Cl[b]/ at.%
NC	0.00	0.00	84.2	9.3	6.4	0.1
AC	0.00	0.00	95.3	0.3	4.4	0.0
Pt/NC-w-473	0.97	0.08	85.8	8.5	5.1	0.6
Pt/NC-w-673	1.00	0.07	84.5	9.1	5.2	0.2
Pt/NC-w-1073	0.94	0.08	87.0	8.4	3.0	0.1
Pt/AC-w-473	0.94	0.06	95.0	0.4	4.2	0.2
Pt/AC-w-1073	0.97	0.04	96.7	0.6	2.6	0.0
Pt/AC-a-473	0.92	0.11	91.9	0.2	7.1	0.8
Pt/AC-a-673	1.02	0.07	95.2	0.1	4.0	0.7
Pt/AC-a-1073	0.97	0.07	96.3	0.0	3.1	0.5
Pt/NC-w-473-12h	0.94	0.10	86.4	8.0	4.3	1.3
Pt/AC-w-473-50h	0.99	0.07	96.6	0.0	3.1	0.9

[a]ICP-EOS.

[b]XPS.